

ORIGINAL RESEARCH

Flower flake-shaped zinc oxide nanoparticles synthesized by microwave technique with different plant extracts for anti-bacterial activity

Nirdosh Verma^{a,b}, Lacy Loveleen^c, Surendra Nimesh^c, Sunil Kumar^e, Kuldeep Kumar^{d,b}, Kamal Jeet^f, Naveen Thakur^{a,b,*}

^aDepartment of Physics, Career Point University, Hamirpur, Himachal Pradesh-176041, India

^bCentre for Nano-Science and Technology, Career Point University, Hamirpur, Himachal Pradesh-176041, India

^cDepartment of Biotechnology, School of Life Sciences, Central University of Rajasthan, Ajmer, Rajasthan-305801, India

^dDepartment of Chemistry, Career Point University, Hamirpur, Himachal Pradesh-176041, India

^eDepartment of Animal Sciences, Central University of Himachal Pradesh, Kangra, Shahpur, Himachal Pradesh 176206, India

^fDepartment of Pharmaceutical Sciences, Career Point University, Hamirpur, Himachal Pradesh-176041, India

* Corresponding author's Email: naveenthakur2327@gmail.com

© The Author(s), 2024

Abstract

Plants are recognized for containing crucial phytochemicals that play a significant role in reducing and capping nanoparticles, contributing to advancements in nanoparticle synthesis. The use of plant extracts as stabilizing agents in nanoparticle synthesis has gained immense popularity in contemporary research. These stabilizing agents also help mitigate the potential toxic effects of chemicals used in the synthesis process. In this study, four distinct plants- *Psidiumguajava*, *Colocasiaesculenta*, *Phyllanthusemblica*, and *Murrayakoenigii* were selected as stabilizers for the synthesis of ZnO nanoparticles using the microwave technique. Various characterization techniques, including X-ray diffraction (XRD), scanning electron microscopy (SEM), energy-dispersive X-ray spectroscopy (EDX), transmission electron microscopy (TEM), UV-Vis spectroscopy, and Fourier-transform infrared spectroscopy (FTIR), were employed to elucidate the morphology, band gap, and functional groups of the synthesized nanoparticles. XRD analysis revealed crystallite sizes of 14 nm for *Psidiumguajava*, 12 nm for *Colocasiaesculenta*, 17 nm for *Phyllanthusemblica*, and 13 nm for *Murrayakoenigii*. The corresponding band gaps were 3.28 eV, 3.33 eV, 3.35 eV, and 3.20 eV, respectively. SEM analysis showed that the nanoparticle shapes resembled flowers. Additionally, the assessment of antibacterial activity against pathogens, along with a comparative study, aids in evaluating the optimal utilization of nanoparticles in industries such as food packaging and cosmetics.

Keywords: *Colocasiaesculenta*; *Murrayakoenigii*; *Phyllanthusemblica*; *Psidiumguajava*; Zinc Oxide

Article History:

Received: 21-Feb-2024

Revised: 04-Oct-2024

Accepted: 28-Nov-2024

Introduction

The development of nanoparticles from various metal salts has significantly advanced the field of health and medicine. The small size of nanoparticles has revolutionized nanotechnology due to their unique properties (Prakasham et al., 2014). In the current era, scientists are keen to use environmentally friendly methods for nanoparticle production, primarily because of their cost-effectiveness and their potential as effective capping and stabilizing agents. This approach reduces reliance on chemicals and minimizes their adverse impacts. Living organisms play a crucial role in the biofabrication of metal oxide nanoparticles. Among all biological sources, plants are considered the best candidates for large-scale biosynthesis of nanoparticles due to the diversity in size and shape of nanoparticles synthesized from them compared to those from other sources (Kumar et al., 2024a). Green synthesis does not require the addition of surfactants or capping agents, as plant metabolites act as stabilizing agents (Rouhi et al., 2013), which is a major advantage over chemical synthesis. Additionally, green synthesis is eco-friendly, simpler, and less costly than chemical methods. Plant extracts are non-toxic and use water as a medium for the preparation of biosynthesized nanoparticles (Kumar et al., 2024b). Recently, researchers across various fields have shown interest in zinc oxide nanoparticles due to their distinctive properties and diverse applications (Baker et al., 2013). Zinc oxide nanoparticles are utilized in both industrial and scientific areas (Kumar et al., 2024c) because of their high excitonic binding energy and wide band gap at the nanoscale. Moreover, the biosynthesis of zinc oxide has a wide range of applications in the biological field, including antibacterial, antifungal, drug delivery, gene delivery, biological sensing, and anti-diabetic activities (Kolodziejczak et al., 2014). In the past decade, numerous studies have reported the biosynthesis of zinc oxide using various plant extracts. Literature reveals that zinc oxide nanoparticles have been synthesized from leaf extracts of *Ocimumbasilicum L. var. purpurascens*, *Partheniumhysterophorus L.* (Kolodziejczak et al., 2014), *Calotropisprocera*, *Aloe vera* (Singhai et al., 1997), *Plectranthusamboinicus* (Kumar et al., 2024d), *Citrus aurantifolia* (Thakur & Thakur, 2024a), *Artocarpusheterophyllus* (Rana et al., 2024), *Laurusnobilis* (Samat et al., 2013), *Annonasquamosa* (Thakur & Thakur, 2024b), and flower extracts of *Anchusaitalica* (Vijayakuma et al., 2016), *Trifoliumpratense* (Thakur et al., 2023), *Punicagranatum* (Azizi et al., 2016); seed extracts of *Pongamiapinnata* (Dobrucka & Dlugaszewska, 2016) and *Cuminumcyminum* (Thakur et al., 2024c); fruit extracts of *Borassusflabellifer* (Malaikozhundan et al., 2017), *Embliaofficinalis* (Zare et al., 2017), and *Artocarpusgoezianus* (Thakur et al., 2024d); root extracts of *Withaniasomnifera* (Anbukkarasi et al., 2015) and *Rubusfairholmianus* (Anitha et al., 2018); and peel extracts of *Musa sapientum* (Prasad et al., 2021) and *Punicagranatum* (Rajendran et al., 2021).

This investigation utilized leaf extracts from four distinct plants to synthesize zinc oxide nanoparticles: *Psidiumguajava*, *Colocasiaesculenta*, *Phyllanthusemblica*, and *Murrayakoenigii*. *Psidiumguajava*, known for its medicinal properties, is associated with various biological activities, including antibacterial, antitussive, and antidiabetic effects (Ruangtong et al., 2021). The other plants also demonstrated antibacterial and antimicrobial activities using different synthesis approaches. Zinc oxide (ZnO) nanoparticles are prized for their diverse applications. Using plant extracts for their synthesis offers a greener, eco-friendly alternative to traditional methods. Plant-based synthesis utilizes natural phytochemicals for reduction and stabilization, enhancing the nanoparticles'

stability and biocompatibility while reducing environmental impact. Zinc oxide nanoparticles were synthesized using microwave techniques with these plant extracts, and the prepared nanoparticles were characterized using XRD, SEM, EDS, TEM, FTIR, and UV-spectroscopy to understand their morphology.

Material and Methodology

Chemicals

To conduct the microwave-assisted synthesis of ZnO nanoparticles and evaluate their antibacterial activity, analytical research-grade Zinc acetate dihydrate ($(\text{CH}_3\text{COOH})_2\text{Zn}\cdot 2\text{H}_2\text{O}$), Sodium hydroxide (NaOH), and Agar-agar Type I, Mueller Hinton broth, Nutrient agar was procured from Sigma. *Escherichia coli* (MTCC 739), *Staphylococcus aureus* (MTCC 737), and *Bacillus subtilis* (MTCC 441) were acquired from CSIR-IMTECH, Chandigarh.

Preparation of Plant Extracts

Fresh leaves of *Psidiumguajava*, *Colocasiaesculenta*, *Phyllanthusemblica* and *Murrayakoenigii* plants were collected from the local area of Hamirpur, Himachal Pradesh. The leaves underwent meticulous chopping and were subsequently washed with tap water, followed by a rinse with distilled water, and finally air-dried. A quantity of 10 g of the dried leaves was then crushed and introduced into 100 ml of distilled water. The plant extract was formulated by boiling the mixture at 80 °C for 1 hour in a Soxhlet apparatus, which was sterilized with ethanol before preparing the plant extract. After cooling, the resultant solutions were filtered with Whatman filter paper to acquire a transparent plant extract solution. These plant extracts were stored in a refrigerator at 4 °C for subsequent experimentation.

Experimental Procedure

For the preparation of zinc oxide nanoparticles, 100 ml of 0.005M zinc acetate dihydrate salt solution was prepared by continuous stirring for 60 minutes on a magnetic stirrer. To synthesize nanoparticles mediated by *Psidiumguajava*, 10 ml of the plant extract was carefully added drop by drop into the salt solution and stirred for 60 minutes. Subsequently, a 2 M NaOH solution was introduced gradually into the mixture to attain a pH level of 12. Thereafter, the solution was placed inside a preheated domestic microwave at 200 °C for 10 min. The resulting precipitates were then cooled and filtered into another vessel for washing. The resulting precipitate underwent 2-3 washes with both distilled water and ethanol. Subsequently, the precipitate was subjected to drying in an oven at 70 °C for 8 hours to yield ZnO nanoparticles. A schematic diagram depicting the green synthesis of ZnO nanoparticles is presented in **Fig1**. The identical procedure was employed for the synthesis of Zinc oxide nanoparticles mediated by plant extracts from *Colocasiaesculenta*, *Phyllanthusemblica*, and *Murrayakoenigii*.

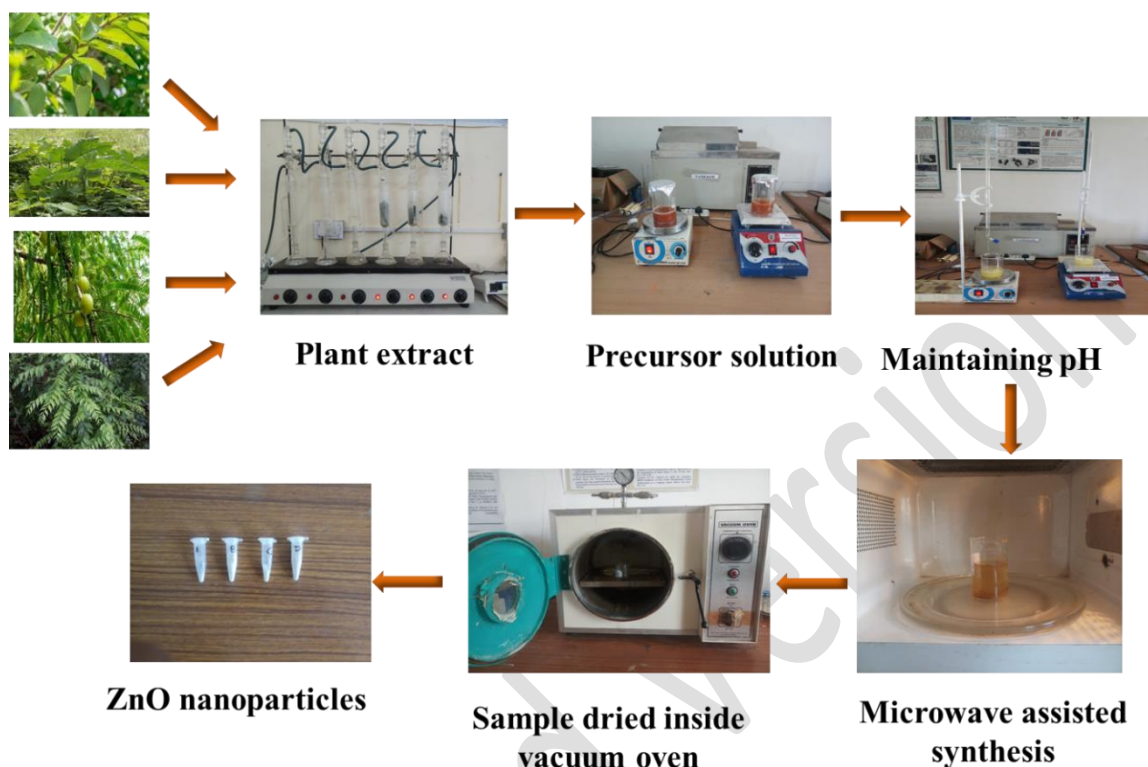


Figure 1. Schematic representation of green synthesis of ZnO nanoparticles using microwave technique

Characterization

The structural features of ZnO nanoparticles formed with different plant extracts were obtained by using an X-ray diffractometer, TEM/SEM, EDS, FTIR, and UV-vis spectrophotometer. The XRD analysis usually provides information regarding the crystalline nature, lattice formation, and crystalline grain size of matter. A radiation source of $\text{CuK}\alpha$ was used to produce X-rays of wavelength, $\lambda = 0.154 \text{ nm}$. A Quanta 2000 microscope was used to record SEM micrographs. Further, EDS (energy dispersive X-ray) has been used to recognize the composition of resultant nanoparticles. TEM, FTIR and UV- spectroscopy have also been performed to understand the morphology, and to identify the compounds and optical properties of synthesized samples. The initial characterization of ZnO nanoparticles of *Psidium guajava*, *Colocasia esculenta*, *Phyllanthus emblica* and *Murrayakoenigii* was performed using a UV-vis spectrophotometer. The technique was used to calculate the bandgap of synthesized nanoparticles at a wavelength range of 200-800 nm present in a suspension. Bandgap and spacing of the electronic level are in an inversely proportional relationship with the size of nanoparticles, the more the bandgap the lesser the size of particles. Such phenomenon is commonly termed as “quantum size effect”. The bandgap energy (E) of the synthesized zinc oxide nanoparticles was calculated utilizing Planck's equation, as expressed in equation (1).

$$E_g = \frac{hc}{\lambda} = \frac{1240}{\lambda} \quad \dots (1)$$

Here, E_g represents the energy bandgap in electron volts (eV), h stands for the Planck constant with a value of 6.626×10^{-34} J/s, c denotes the speed of light equal to 3×10^8 m/s, and λ_{\max} signifies the maximum absorption wavelength measured in nanometers (nm).

Antibacterial activity of ZnO nanoparticles

The agar well diffusion method was employed to evaluate the antimicrobial characteristics of ZnO nanoparticles synthesized through green methods. Three different concentrations of each of the four nanoparticle types were examined to assess their efficacy as antibacterial agents against one Gram-negative bacterium (*Escherichia coli*) and two Gram-positive bacteria (*Bacillus subtilis* and *Staphylococcus aureus*) (Sukri et al., 2019). To culture bacteria, first prepare and sterilize a growth medium, such as nutrient agar or broth, through autoclaving. Inoculate the medium with the bacterial sample using a sterile loop or pipette. Incubate the inoculated medium at 35-37°C for 18-24 hours, or as required for the specific bacterial strain. After incubation, evaluate bacterial growth by inspecting for colonies on agar plates or turbidity in liquid cultures. For isolation and further study, streak colonies onto fresh agar plates to obtain pure cultures. Store cultures long-term via freezing and short-term in a refrigerator.

Result and Discussion

XRD Analysis

XRD was performed to confirm the existence of ZnO nanoparticles along with their structural parameters. The XRD patterns corresponding to Zinc oxide nanopowders synthesized with four different plant extracts by microwave technique are displayed in **Fig. 2**. The information provided in x-ray peaks helps to obtain crystallite aspects. Similar patterns are exhibited in all four samples. Reflected planes (100), (002), (101), (102), (110), (103), (112) and (201) correspond to Bragg angle's 31.9° , 34.5° , 36.3° , 47.6° , 56.7° , 62.9° , 68.1° and 69.1° are indicating toward ZnO hexagonal structure. These results are compared with JCPDS 36-1541 (Rehan et al., 2019) that were reported in previous literature. Maximum intensity of the (101) plane in all four samples assures the materialization of the hexagonal wurtzite structure.

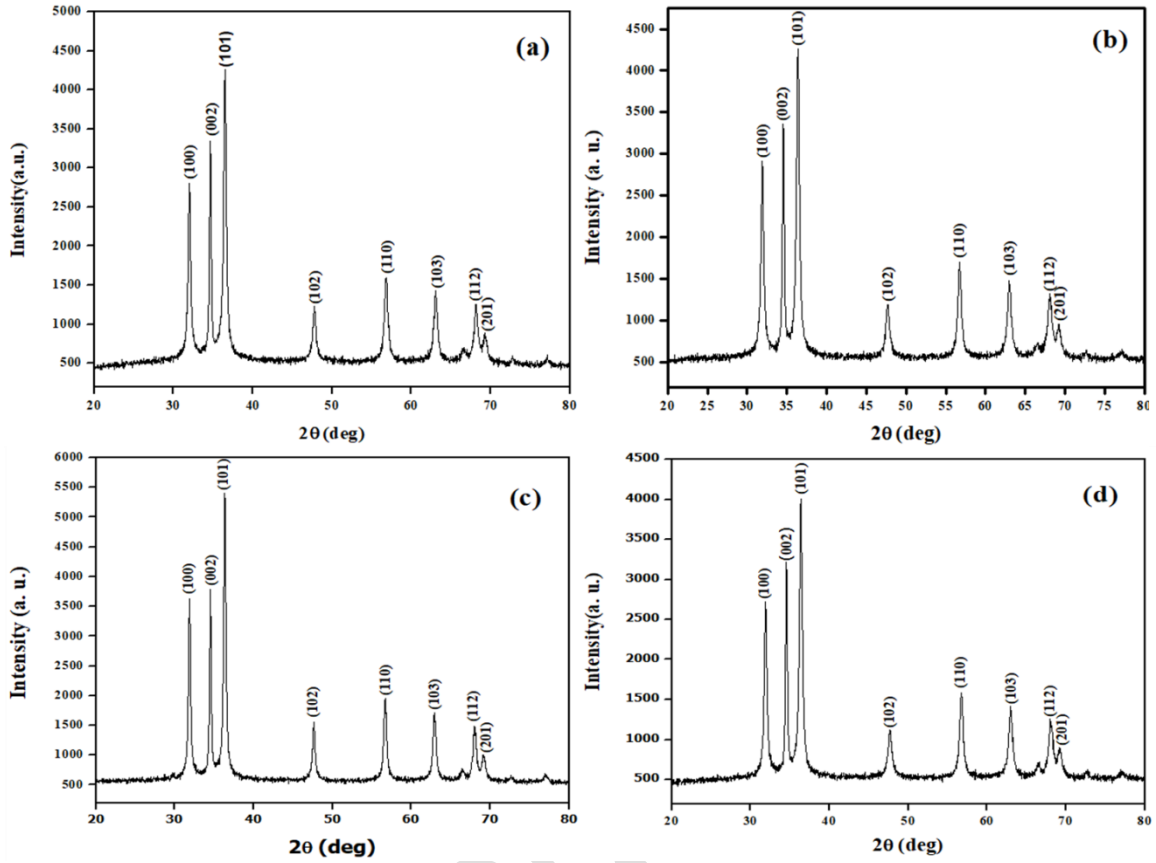


Figure 2. XRD peaks specifying the existence of ZnO. (a) *Psidiumguajava*, (b) *Colocasiaesculenta*, (c) *Phyllanthusemblica* and (d) *Murrayakoenigii*, leaves directed ZnO nanoparticles

The ZnO structural parameters such as lattice parameters ($a=b$, c), degree of crystallinity (χ^c) (Sharma et al., 2021), crystallite size (D) (Sun et al., 2011), microstrain (ϵ) (Ren et al., 2009), stacking fault (α) (and Dislocation density (δ)) [33] are calculated by using empirical relations are mentioned as follow:

$$a = b = (\lambda / (3^{1/2} \sin \theta))$$

$$c = (\lambda / \sin \theta)$$

$$\chi^c = (0.24 / \beta)^3$$

$$D = 0.9 \lambda / \beta \cos \theta$$

$$\epsilon = \beta / 4 \tan \theta$$

$$\alpha = \left(\frac{2\pi^2}{45(3 \tan \theta)^{1/2}} \right) \beta$$

$$\delta = 1 / (D)^2$$

Whereas λ , θ and β represent x-ray wavelength, Bragg's angle and FWHM (Full width at half maxima). **Table 1** provides calculated structural parameters by using XRD data and above mention empirical relations.

Table 1. Calculated results for structural parameters by using XRD data

S.No	Structural parameters	Samples	2θ (deg)	FWHM (β)	Formula Used	Results
1	a(Å)	(a)	31.09	0.31	$(\lambda/(3^{1/2}\sin\theta))$	3.20 nm
		(b)		0.32		
		(c)		0.28		
		(d)		0.32		
2	c(Å)	(a)	34.5	0.31	$(\lambda/\sin\theta)$	5.12 nm
		(b)		0.32		
		(c)		0.28		
		(d)		0.32		
3	χ^c	(a)	34.5	0.31	$(0.24/\beta)^3$	0.464
		(b)		0.32		0.421
		(c)		0.28		0.629
		(d)		0.32		0.421
4	D(nm)	(a)	36.3	0.45	$0.9 \lambda/\beta \cos\theta$	14.22 nm
		(b)		0.5		12.80 nm
		(c)		0.37		17.30 nm
		(d)		0.49		13.06 nm
5	ε	(a)	36.3	0.45	$\beta/4\tan\theta$	6.44×10^{-4}
		(b)		0.5		7.15×10^{-4}
		(c)		0.37		5.29×10^{-4}
		(d)		0.49		7.01×10^{-4}
6	α	(a)	36.3	0.45	$(\frac{2\pi^2}{45(3\tan\theta)^{1/2}}) \beta$	0.199206
		(b)		0.5		0.22134
		(c)		0.37		0.163792
		(d)		0.49		0.216914

Table 2. Calculated results for Dislocation density for samples by using XRD data

S. No	Samples	2θ (deg)	FWHM (β)	D (nm)	Formula Used	Δ
01	(a)	36.3	0.45	14.22 nm	$1/(D)^2$	4.94×10^{-3}
02	(b)		0.5	12.80 nm		6.10×10^{-3}
03	(c)		0.37	17.30 nm		3.34×10^{-3}
04	(d)		0.49	13.06 nm		5.86×10^{-3}

Dislocation density (δ) has also been calculated which is mentioned in **Table 2**. Strain represents imperfection or defect in a crystal with the arrangement of lattice constants (Karthik et al., 2020). Bond length changes due to the variation in lattice constant that results in strain and charge carrier gradient responsible for the shrinkage of the crystallite in the crystal structure (Mobarak et al., 2022). The lower value of strain in sample (c) suggests that zinc oxide nanoparticles synthesized with *Phyllanthusemblica* have more crystallinity as compared to other samples which can also be seen in the values of degree of crystallinity.

SEM and EDAX Analysis

Scanning Electron Microscopy is performed to understand the morphology of synthesized Zinc oxide with different plant extracts. **(Fig.3)** shows SEM results for all synthesized samples. **Fig.3 (a-d)** indicates that pure Zinc oxide

samples prepared by microwave technique have flower flake shapes and are abundantly distributed regularly. The average flower size was calculated as 637 nm for sample A, 282 nm for sample B, 813 nm for sample C and 735 nm for sample D by using ImageJ software from SEM results. The variation in average sizes of samples is due to the usage of different plant extracts. Also, there is no contact of nanoparticles with each other in samples, which indicates the stability of particles by reducing agent (Bindu et al., 2014).

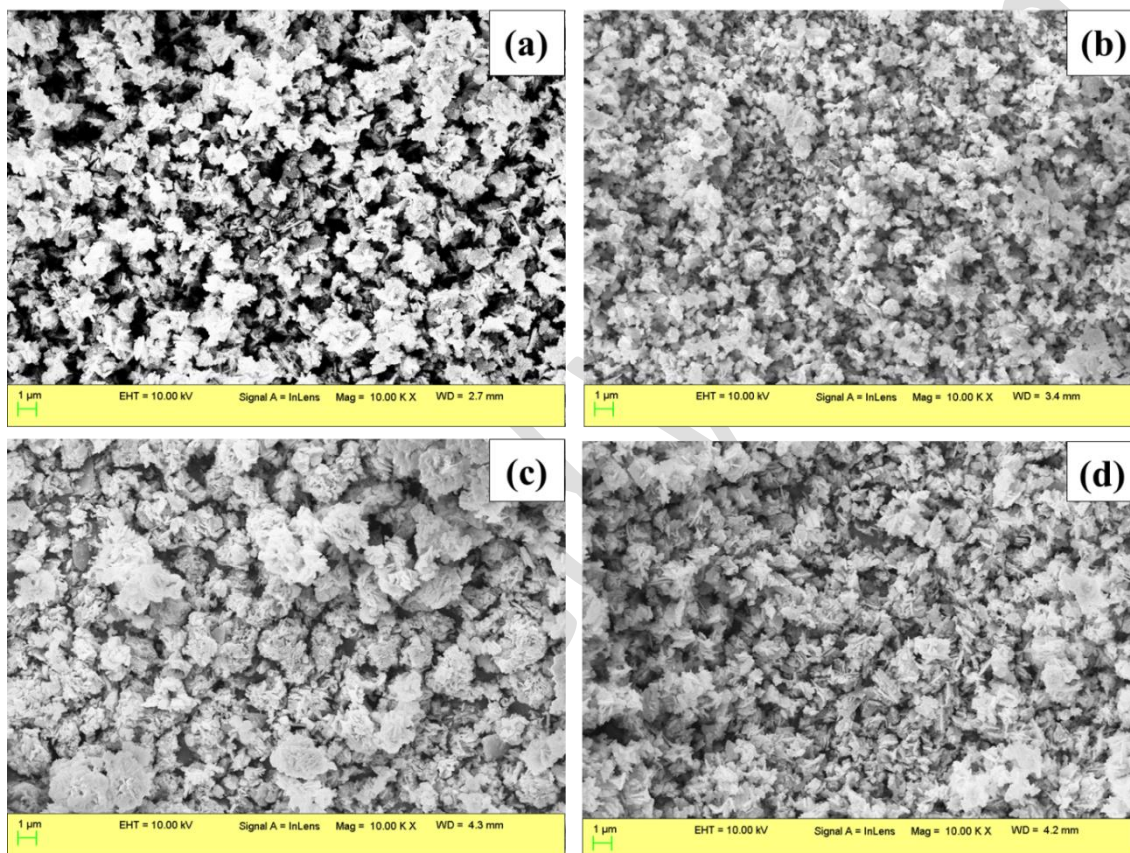


Figure 3. SEM images for synthesized ZnO nanoparticles with (a) *Psidium guajava*, (b) *Colocasia esculenta*, (c) *Phyllanthus emblica* and (d) *Murrayakoenigii*

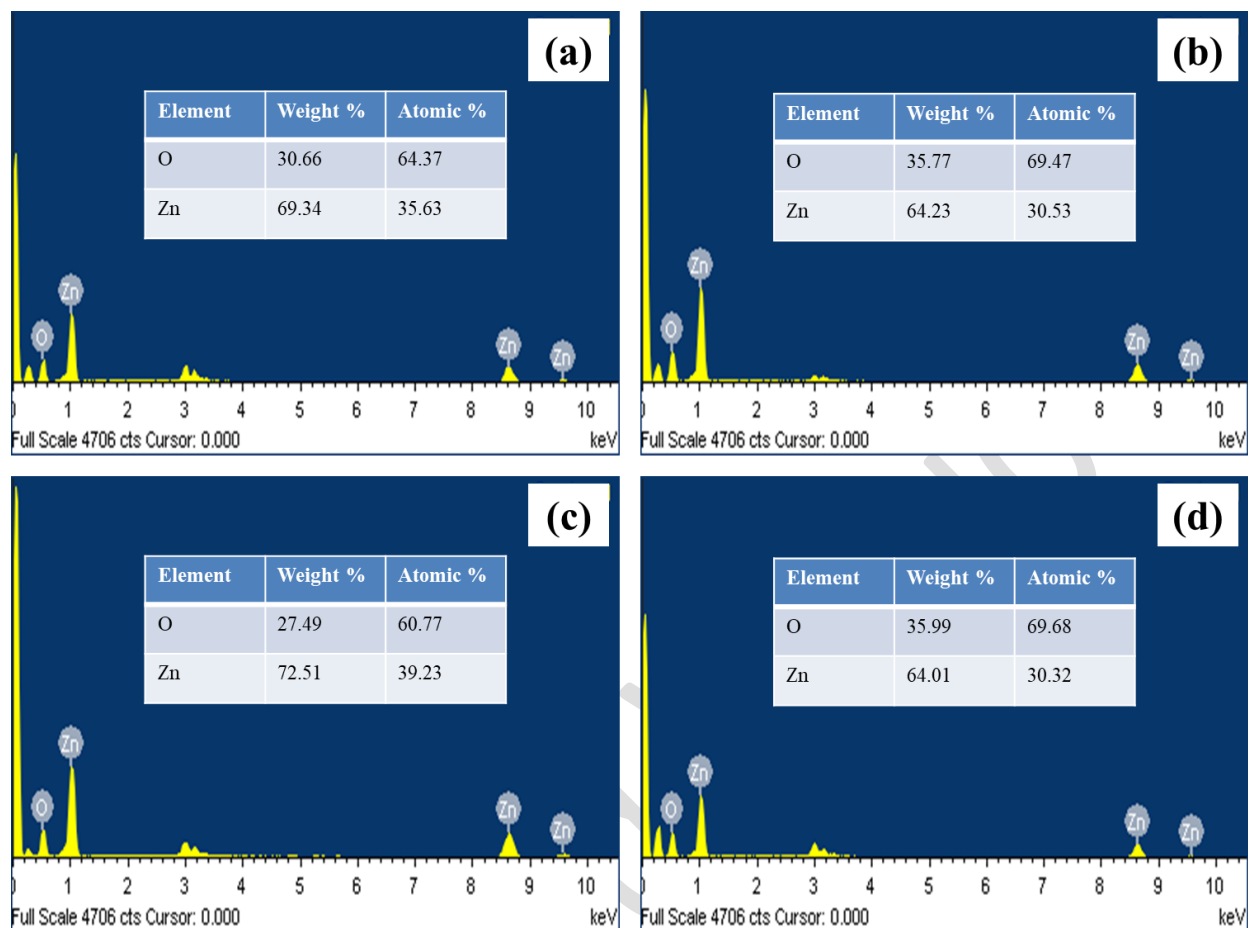


Figure 4.EDAX graphs with elemental composition for samples. **(a)***Psidiumguajava*, **(b)***Colocasiaesculenta*, **(c)***Phyllanthusemblica* and **(d)***Murraya*

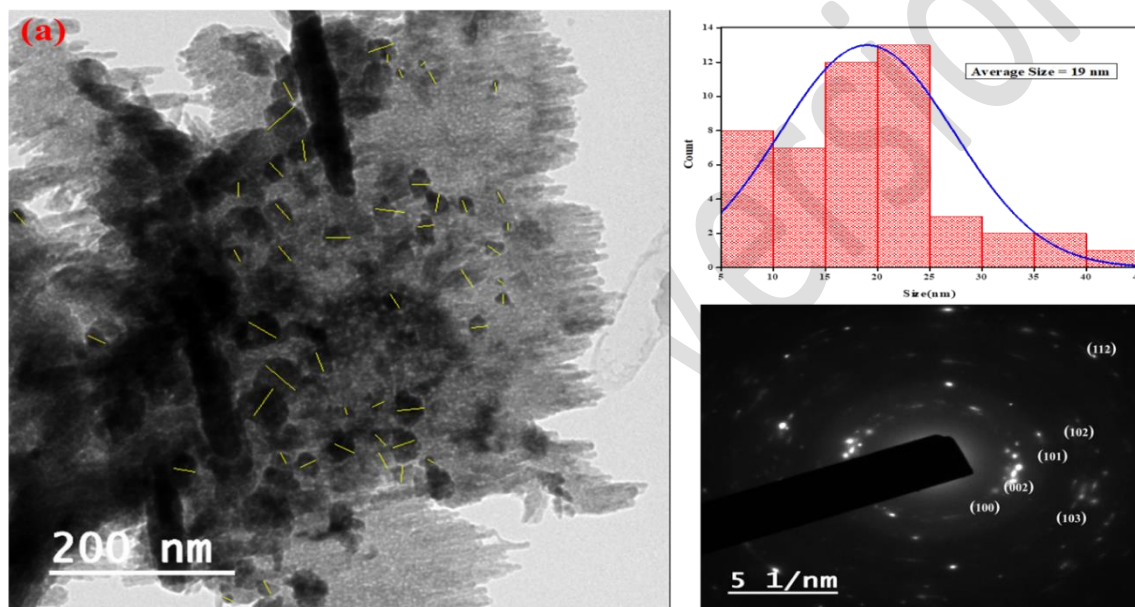
The Energy-dispersive X-ray analysis has also been performed for all synthesized samples as shown in **(Fig.4)**. This analysis is done to know the atomic as well as weight percentage of elements present in samples. **(Fig.4)** confirms the presence of pure Zinc oxide of Zn and O elements without any impurity, whose atomic and weight percentages are also given in tabular format.

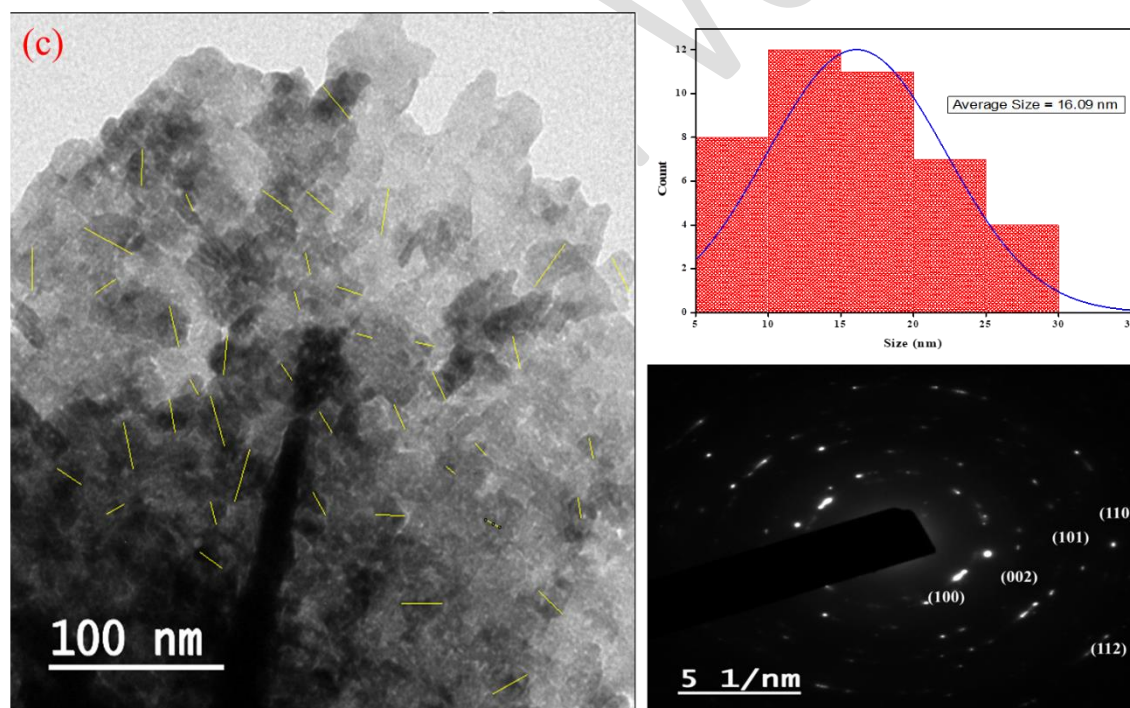
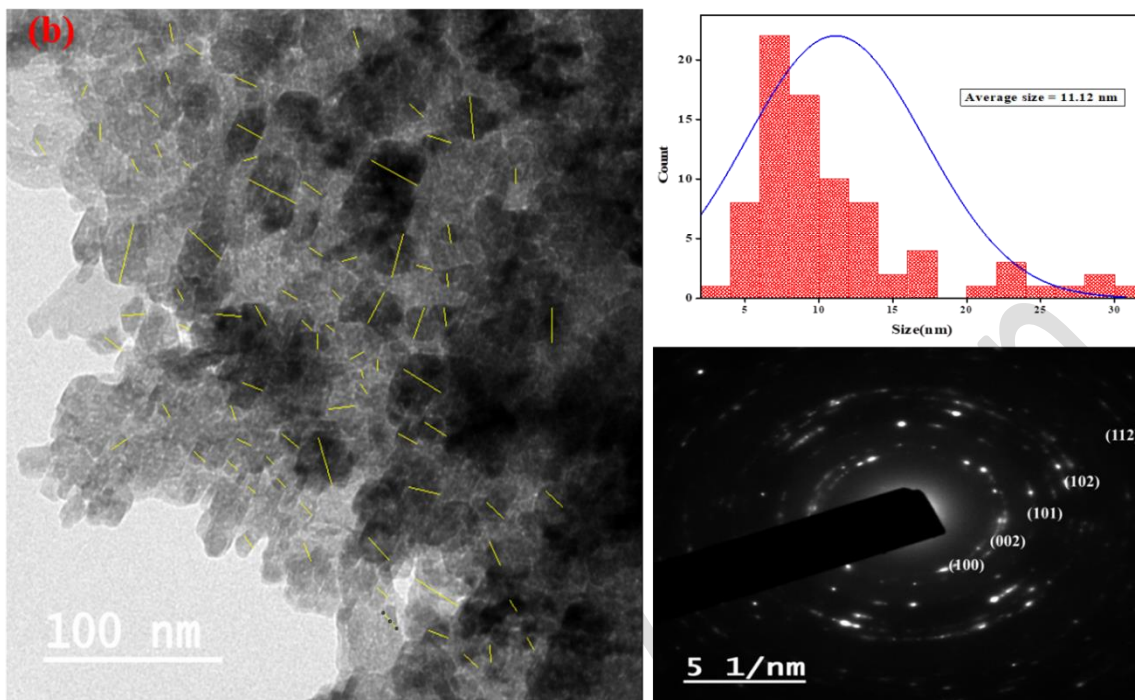
TEM

TEM images in Fig.5 (a-d) of synthesized ZnO nanoparticles with *Psidiumguajava*, *Colocasiaesculenta*, *Phyllanthusemblica*, and *Murrayakoenigii* reveal that the nanoparticles exhibit irregular shapes, including spherical ones. Displayed histograms in **Fig.5(a- d)** help to determine the average size of nanoparticles as shown in **Table 3**. The average particle sizes for samples (a), (b), (c), and (d) were 19 nm, 15.12 nm, 16.09 nm, and 23.81 nm, respectively, as determined using ImageJ software. Variations in particle size were observed due to the use of different plant extracts.

Table 3. Exploration of histograms displayed in **Fig. 3 (a-d)**

S. No.	Sample (a), (b), (c) & (d)	Size of nanoparticles (range)	Maximum distribution of nanoparticles (range)	Average size (nm)
01	ZnO - <i>Psidiumguajava</i>	05 – 45 nm	15 – 25 nm	19 nm
02	ZnO - <i>Colocasiaesculenta</i>	05 – 30 nm	05 – 10 nm	15.12 nm
03	ZnO - <i>Phyllanthusemblica</i>	05 – 35 nm	10 – 20 nm	16.09 nm
04	ZnO - <i>Murrayakoenigii</i>	10 – 90 nm	10 – 30 nm	23.81 nm





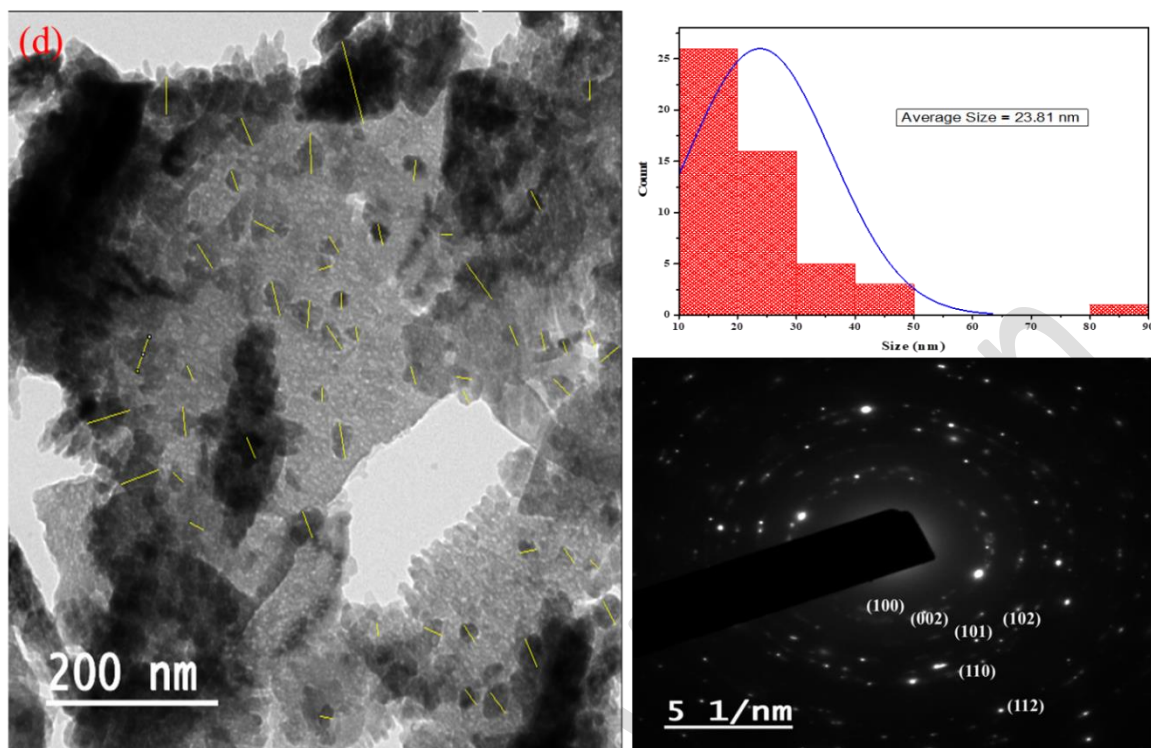


Figure 5. TEM and SAED images for samples. (a) *Psidium guajava*, (b) *Colocasia esculenta*, (c) *Phyllanthus emblica* and (d) *Murrayakoenigii*

Moreover, SAED (Selected Area Electron Diffraction) patterns for all synthesized samples are displayed in **Fig. 5 (a-d)**. ImageJ software is used to calculate the estimated inter-planer distance or d-spacing as displayed in supplementary information as **Table 4**, where r represents the radius of concentric circles that have been plotted in the SAED pattern.

Table 4. Comparison of calculated d-spacing of all samples with reported results

Hexagonal wurtzite ZnO (JCPDS No. 00-036-1451)		Sample (a)			Sample (b)		
(hkl)	d(A ⁰)	1/2r	r (nm)	d-spacing	1/2r	r (nm)	d-spacing
100	2.81430	7.121	0.280859	2.808594	7.101	0.28165	2.816505
002	2.60332	7.688	0.260146	2.601457	7.683	0.260315	2.60315
101	2.47592	8.051	0.248416	2.484163	8.051	0.248416	2.484163
102	1.91114	10.448	0.191424	1.914242	10.508	0.190331	1.903312
103	1.47712	13.726	0.145709	1.457089	-	-	-
112	1.37818	14.559	0.137372	1.373721	14.559	0.137372	1.373721
Hexagonal wurtzite ZnO (JCPDS No. 00-036-1451)		Sample (c)			Sample (d)		
(hkl)	d(A ⁰)	1/2r	r (nm)	d-spacing	1/2r	r (nm)	d-spacing
100	2.81430	6.998	0.285796	2.857959	7.078	0.282566	2.825657
002	2.60332	7.678	0.260485	2.604845	7.708	0.259471	2.594707
101	2.47592	8.151	0.245369	2.453687	8.051	0.248416	2.484163
102	1.91114	-	-	-	10.521	0.190096	1.90096
110	1.62472	12.208	0.163827	1.63827	12.298	0.162628	1.626281
112	1.37818	14.609	0.136902	1.369019	14.592	0.137061	1.370614

FTIR Analysis

The synthesized zinc oxide nanoparticles have been examined in the range of 4000-600 cm^{-1} to ensure the appearance of functional groups through the FTIR spectrum, as shown in **Fig.6**. It has been observed that strong broad peaks of O-H stretching lie between 3550 and 3200 cm^{-1} in all samples (Koutu et al., 2016). Furthermore, in all synthesized samples, a robust stretching of O=C=O appeared at 2359 cm^{-1} for sample (a), 2351 cm^{-1} for sample (b), 2352 cm^{-1} for sample (c), and 2359 cm^{-1} for sample (d), respectively, attributable to the presence of CO_2 in the air. Peaks at 1571 cm^{-1} in sample (b) and 1578 cm^{-1} in sample (d) corresponded to C=C stretching (cyclic alkene). Within the range of 1420 to 1330 cm^{-1} , peaks indicative of O-H bending (alcohol) were observed in all samples. The broader and weaker bands, located near 900 cm^{-1} in sample (a), 902 cm^{-1} in sample (b), 867 cm^{-1} in sample (c), and 874 cm^{-1} in sample (d), represented N-H bending vibrations of amines [Song et al., 2008; Farzana et al., 2015]. The results show a range of peak absorptions below 850 cm^{-1} . Specifically, the peak near 664 cm^{-1} is commonly linked to bending vibrations of hydroxyl (O-H) groups or possibly to bending vibrations of C-H bonds in alkanes (MaslowskyJr, 2019). Likewise, the peak at 671 cm^{-1} may also correspond to bending vibrations of O-H or C-H bonds (Kloprogge et al., 2004). These peaks might reflect specific interactions or bonding within the sample, such as metal-oxygen bonds in metal oxides or other complex structures.

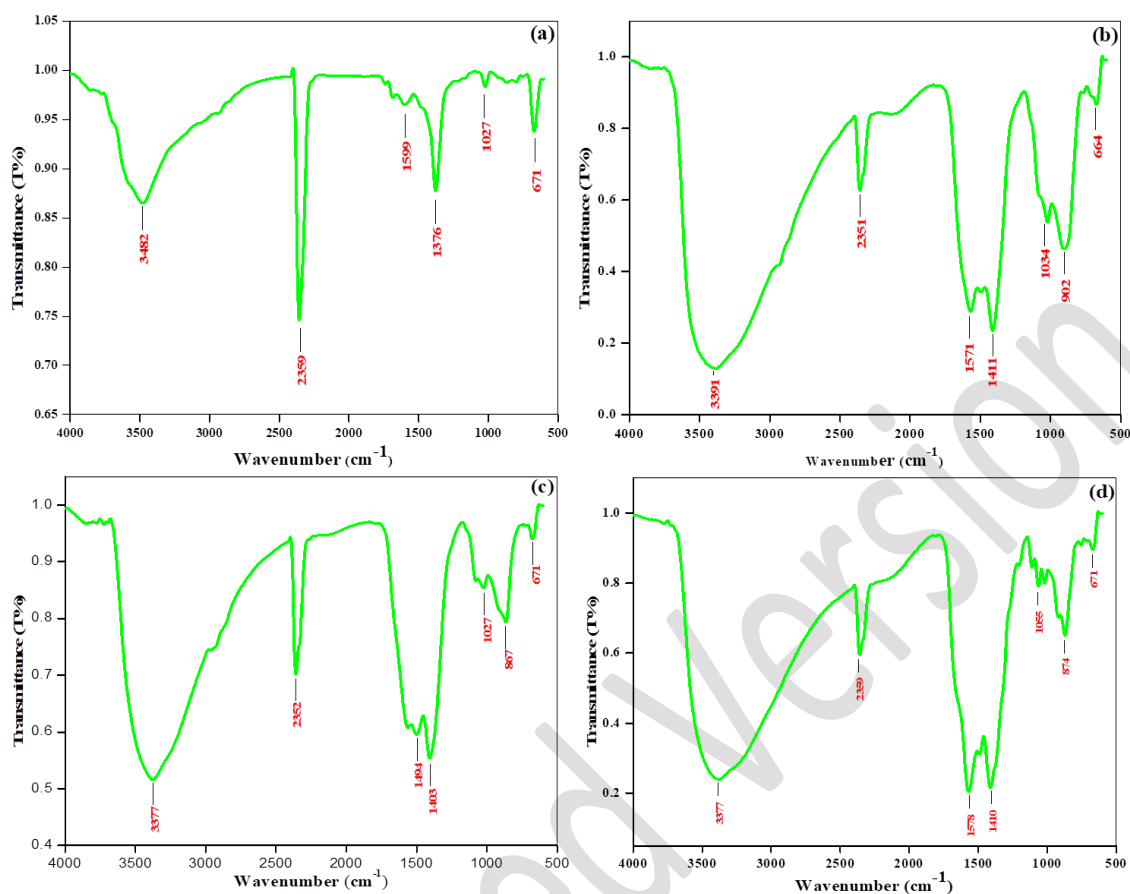


Figure 6. FTIR graphs for samples. (a) *Psidium guajava*, (b) *Colocasia esculenta*, (c) *Phyllanthus emblica* and (d) *Murrayakoenigii*.

UV-Vis Spectroscopy

The bandgap values for the synthesized zinc oxide nanoparticles were determined as 3.28, 3.33, 3.35, and 3.20 eV for *Psidium guajava*, *Colocasia esculenta*, *Phyllanthus emblica*, and *Murrayakoenigii*, respectively, as depicted in **Fig. 7**. Sample's forbidden energy gap determined using the Tauc plot (Verma et al., 2024). Absorbance is subject to modification based on various factors, including particle size and the presence of oxygen deficiencies within the synthesized material (Pai et al., 2019) as shown in **Fig. 8**.

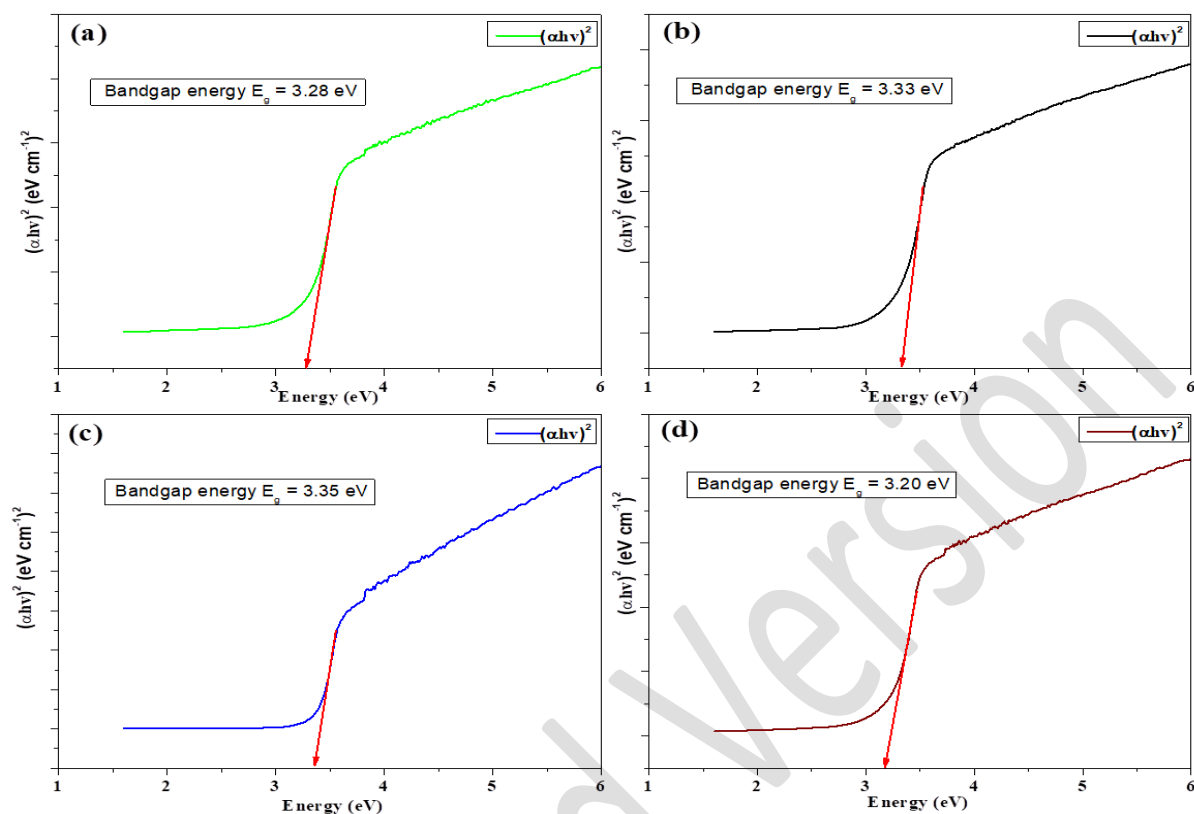


Figure 8. Band gap for samples (a)*Psidiumguajava*, (b)*Colocasiaesculenta*, (c)*Phyllanthusemblica* and (d)*Murrayakoenigii*

Absorbance is subject to modification based on various factors, including particle size and the presence of oxygen deficiencies within the synthesized material (Pai et al., 2019) as shown in **Fig.8**. Changes in the valence band edge toward the lower side and the conduction band edge toward the upper side can occur, leading to interactions between s-d and p-d exchange, resulting in an increased bandgap (Mirza et al., 2019). These structural modifications can alter the mass density, resulting in diverse electronic configurations. UV absorbance spectra indicate that the synthesized zinc oxide nanoparticles function as catalysts under UV light, generating OH radicals with the potential to create a charge for bacterial elimination during antibacterial activity (Dadi et al., 2019).

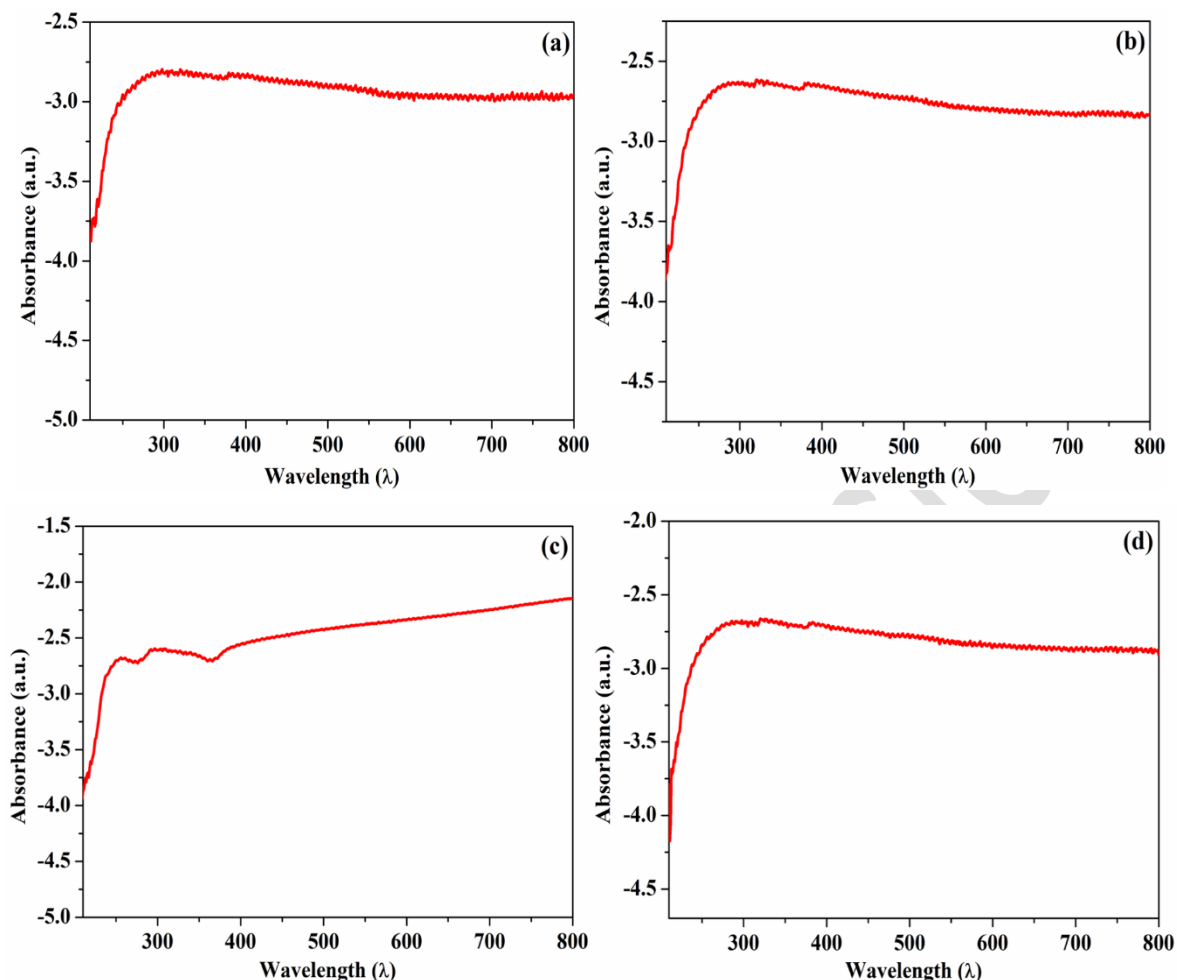


Figure 7. UV spectra for samples (a) *Psidiumguajava*, (b) *Colocasiaesculenta*, (c) *Phyllanthusemblica* and (d) *Murrayakoenigii*

Antibacterial Activity

The good diffusion method was employed to investigate the antibacterial activity of the synthesized nanoparticles against Gram-positive bacteria (*Bacillus subtilis* and *Staphylococcus aureus*) and Gram-negative bacteria (*Escherichia coli*) (Saha et al., 2018). To assess antibacterial activity using the good diffusion method, begin by preparing a Mueller-Hinton agar plate and allowing it to solidify. Inoculate the surface of the agar with a standardized bacterial suspension to create an even bacterial lawn. Once the plate is inoculated, use a sterile cork borer or similar tool to create wells in the agar. Add the synthesized NPs, in specific ratios, into these wells. Incubate the plate at 35-37°C for 18-24 hours to promote bacterial growth. After incubation, observe and measure the clear zones of inhibition around each well. These zones indicate the effectiveness of the test substance, with larger zones reflecting greater antibacterial activity. (Fig. 8) clearly illustrates the observed zone of inhibition for all synthesized samples at varying low concentrations (5, 15, and 25 mg/ml).

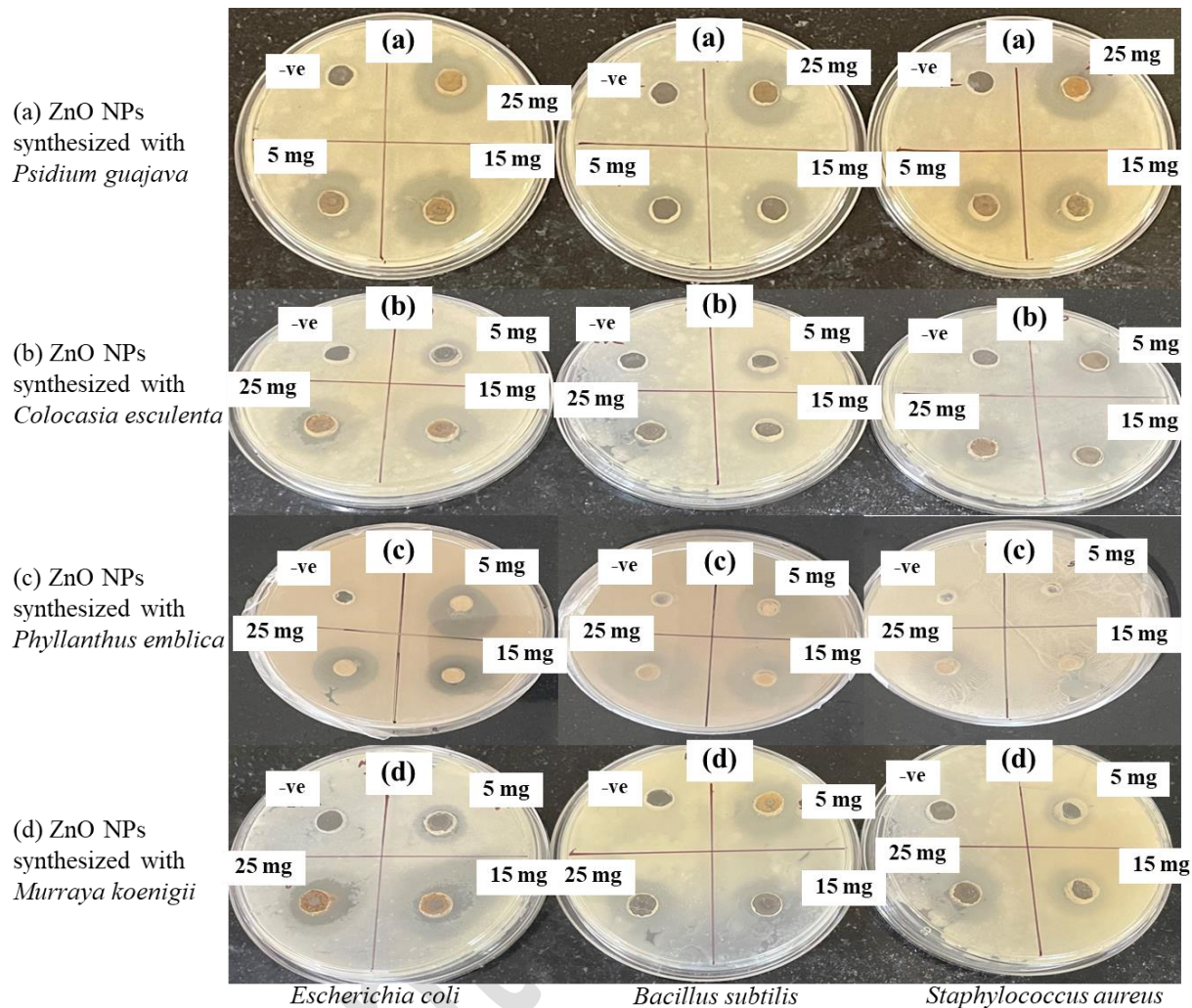


Figure 8. The Zone of inhibition of nanoparticles corresponds to different bacterial strains. (a) *Psidium guajava*, (b) *Colocasia esculenta*, (c) *Phyllanthus emblica* and (d) *Murraya koenigii*

Sample (a) exhibited the highest and most consistent antibacterial effectiveness, with significant zones of inhibition observed across all concentrations, showing a peak activity at 25 mg/ml. In contrast, sample (b) displayed greater variability; although inhibition increased with concentration, the activity at lower concentrations was notably less effective. Sample (c) showed moderate activity, with increasing inhibition at higher concentrations but generally lower effectiveness compared to sample (a). Sample (d) had the least overall antibacterial activity, with lower zones of inhibition at all tested concentrations. These findings indicate that the synthesis conditions and concentration of ZnO NPs greatly influence their antibacterial efficacy, with sample (a) providing the most pronounced and consistent results. Higher efficiency for antibacterial activity is also seen in previous literature (Saha et al., 2018; Ramya et al., 2022).

Table 5. Comparison of ZOI of all samples at different concentrations against Gram-positive and Gram-negative bacteria

Synthesized ZnO NPs samples	Bacteria	Nanoparticle concentration (mg/ml)	ZOI (Zone of Inhibition) (mm)
(a)	<i>Escherichia coli</i>	5	18
		15	17
		25	18
	<i>Bacillus subtilis</i>	5	14
		15	18
		25	24
	<i>Staphylococcus aureus</i>	5	15
		15	19
		25	24
(b)	<i>Escherichia coli</i>	5	08
		15	16
		25	24
	<i>Bacillus subtilis</i>	5	08
		15	15
		25	22
	<i>Staphylococcus aureus</i>	5	09
		15	17
		25	23
(c)	<i>Escherichia coli</i>	5	10
		15	18
		25	24
	<i>Bacillus subtilis</i>	5	10
		15	17
		25	23
	<i>Staphylococcus aureus</i>	5	06
		15	08
		25	10
(d)	<i>Escherichia coli</i>	5	08
		15	16
		25	20
	<i>Bacillus subtilis</i>	5	10
		15	14
		25	16
	<i>Staphylococcus aureus</i>	5	06
		15	10
		25	18

The mechanisms of production of oxidative species due to the introduction of metal oxides inside the bacterial cells and the damage to the bacterial cell wall can be found in previous literature (Qidwai et al., 2018). However, there are three possible steps in the antibacterial activity mechanism: (i) formation of ROS (reactive oxygen species), (ii) damage of the cell wall, and (iii) ion reduction (Siddiqi et al., 2018 ; Elumalai et al., 2015). Mechanism of antibacterial activity of synthesized nanoparticles as shown in **Fig. 9**. ZnO nanoparticles exhibit antibacterial activity through

several mechanisms: they generate reactive oxygen species (ROS) that damage bacterial cells, directly disrupt cell membranes, release Zn²⁺ ions that interfere with bacterial processes, and exhibit photocatalytic activity under UV light to produce additional ROS. Their high surface area also enhances their reactivity and interaction with bacterial cells, contributing to their overall antimicrobial effectiveness. Higher efficiency and smaller nanoparticle sizes can exhibit higher antibacterial activity. The antibacterial results have been compared with previous studies involving *Escherichia coli* and *Staphylococcus aureus* pathogens tested against ZnO nanoparticles synthesized through green and chemical methods, as detailed in **Table 6**. From this analysis, we conclude that our synthesized ZnO nanoparticles can be used as food packing material to inhibit bacterial growth and keep food hygienic for a long time.

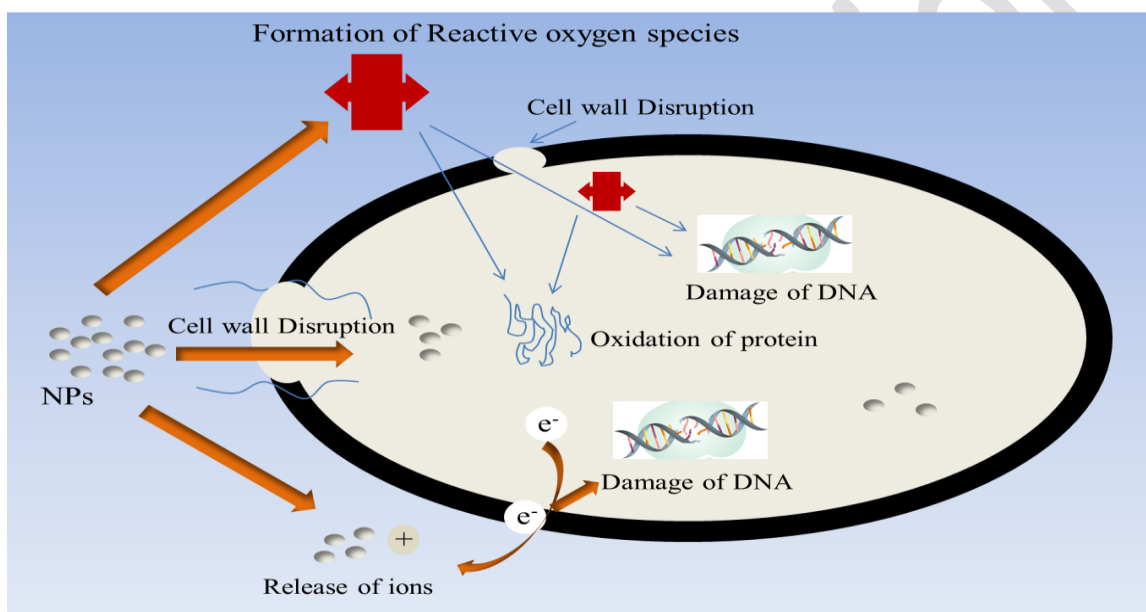


Figure 9. Mechanism for Antibacterial activity of synthesized nanoparticles

Table 6. Comparison of ZOI of present work with literature

S. No.	Pathogens	Synthesized method	Plant extract	Crystallite size (nm)	Concentration of ZnO NPs	ZOI (mm)	References
01	<i>Staphylococcus aureus</i>	Chemical method	<i>Tamarindusindica</i>	19-37 nm	200 mg/l	13.1 ± 0.28	(Rajabi et al., 2017)
02	<i>Staphylococcus aureus</i>	Green method	<i>Suaedaegyptica</i>	60 nm	10 mg/ml	16.01	(Mahendra et al., 2017)
03	<i>Escherichia coli</i>	Green method	<i>Cochlospermum religiosum</i>	7 nm	1 mg/disc	19.36	(Madan et al., 2016)
04	<i>Staphylococcus aureus</i>	Green method	<i>Cochlospermum</i>	7 nm	1 mg/disc	22.20	

			<i>religiosum</i>				
05	<i>Bacillus subtilis</i>	Microwave-assisted green approach	<i>Psidiumguajva</i>	14.22 nm	25 mg/ml	30	Present work
	<i>Staphylococcus aureus</i>						
	<i>Escherichia coli</i>		<i>Murrayakoeni gii</i>	13.09 nm		16	

Conclusion

In this study, we have mentioned the microwave technique for the synthesis of flower-shaped ZnO nanoparticles using four different plant extracts. Plant extracts as stabilizers reduced the crystallite size of synthesized samples, and hence we have reported the size of samples in the range of 12–17 nm through XRD analysis. The flower flake shapes of samples were confirmed by SEM and TEM analysis further helped to understand the morphology of the samples. FTIR analysis confirms the presence of functional groups inside the nanoparticles, which help enhance the antibacterial strength of nanoparticles. Moreover, the band-gap of nanoparticles was calculated with the analysis of UV-vis spectroscopy and found to be 3.34, 3.52, 3.35, and 3.33, which correspond to *Psidiumguajava*, *Colocasiaesculenta*, *Phyllanthusemblica*, and *Murrayakoeni* leaf extracts. The present work can be utilized by the food packaging industry with effective results in antibacterial activity. Moreover, the efficiency of synthesized nanoparticles can be increased by adding dopants for multiple applications.

Ethical Approval

Not required

Consent to Participate

Not required

Consent to Publish

Not required

Authors Contributions

Conception and design of the study: N. Verma, N. Thakur

Acquisition of data: N. Verma, N. Thakur

Analysis and/or interpretation of data: N. Verma, L. Loveleen, S. Nimesh, N. Thakur

Drafting the manuscript: N. Verma, L. Loveleen, K. Jeet, N. Thakur

Revising the manuscript critically for important intellectual content: S. Nimesh, N. Thakur

Approval of the version of the manuscript to be published: Nirdosh Verma, Lacy Loveleen, Surendra Nimesh, Kamal Jeet and Naveen Thakur

Funding

No funding

Conflict of Interest

The authors declare no competing financial interest

Availability Statement

Data will be made available on request

References

- Anbukkarasi, V., Srinivasan, R., &Elangovan, N. (2015). Antimicrobial activity of green synthesized zinc oxide nanoparticles from *Embllicaofficinalis*. *Int. J. Pharm. Sci. Rev. Res*, 33(2), 110-115.
- Anitha, R., Ramesh, K. V., Ravishankar, T. N., Kumar, K. S., &Ramakrishnappa, T. (2018). Cytotoxicity, antibacterial and antifungal activities of ZnO nanoparticles prepared by the *Artocarpusgomezianus* fruit mediated facile green combustion method. *Journal of Science: Advanced Materials and Devices*, 3(4), 440-451. <https://doi.org/10.1016/j.jsamd.2018.11.001>
- Azizi, S., Mohamad, R., Bahadoran, A., Bayat, S., Rahim, R. A., Ariff, A., &Saad, W. Z. (2016). Effect of annealing temperature on antimicrobial and structural properties of bio-synthesized zinc oxide nanoparticles using flower extract of *Anchusaitalica*. *Journal of Photochemistry and Photobiology B: Biology*, 161, 441-449. <https://doi.org/10.1016/j.jphotobiol.2016.06.007>
- Baker, S., Rakshith, D., Kavitha, K. S., Santosh, P., Kavitha, H. U., Rao, Y., &Satish, S. (2013). Plants: emerging as nanofactories towards facile route in synthesis of nanoparticles. *BioImpacts: BI*, 3(3), 111. doi: 10.5681/bi.2013.012
- Bindu, P., & Thomas, S. (2014). Estimation of lattice strain in ZnO nanoparticles: X-ray peak profile analysis. *Journal of Theoretical and Applied Physics*, 8, 123-134. <https://doi.org/10.1007/s40094-014-0141-9>
- Dadi, R., Azouani, R., Traore, M., Mielcarek, C., &Kanaev, A. (2019). Antibacterial activity of ZnO and CuO nanoparticles against gram positive and gram negative strains. *Materials Science and Engineering: C*, 104, 109968. <https://doi.org/10.1016/j.msec.2019.109968>
- Dobrucka, R., &Długaszewska, J. (2016). Biosynthesis and antibacterial activity of ZnO nanoparticles using *Trifoliumpratense* flower extract. *Saudi journal of biological sciences*, 23(4), 517-523. <https://doi.org/10.1016/j.sjbs.2015.05.016>
- Elumalai, K., Velmurugan, S., Ravi, S., Kathiravan, V., &Ashokkumar, S. (2015). RETRACTED: Facile, eco-friendly and template free photosynthesis of cauliflower like ZnO nanoparticles using leaf extract of *Tamarindusindica* (L.) and its biological evolution of antibacterial and antifungal activities. <https://doi.org/10.1016/j.saa.2014.09.129>
- Farzana, M. H., &Meenakshi, S. (2015). Visible light-driven photoactivity of zinc oxide impregnated chitosan beads for the detoxification of textile dyes. *Applied Catalysis A: General*, 503, 124-134. <https://doi.org/10.1016/j.apcata.2014.12.034>
- Hossain, M. S., Mahmud, M., Mobarak, M. B., & Ahmed, S. (2022). Crystallographic analysis of biphasic hydroxyapatite synthesized by different methods: an appraisal between new and existing models. *Chemical Papers*, 1-13. <https://doi.org/10.1007/s11696-021-01949-5>
- Karthik, K., Pushpa, S., Naik, M. M., &Vinuth, M. (2020). Influence of Sn and Mn on structural, optical and magnetic properties of spray pyrolysedCdS thin films. *Materials Research Innovations*. <https://doi.org/10.1080/14328917.2019.1597436>

- Koutu, V., Shastri, L., & Malik, M. M. (2016). Effect of NaOH concentration on optical properties of zinc oxide nanoparticles. *Materials Science-Poland*, 34(4), 819-827. DOI: 10.1515/msp-2016-0119
- Kloprogge, J. T., Hickey, L., & Frost, R. L. (2004). FT-Raman and FT-IR spectroscopic study of synthetic Mg/Zn/Al-hydroxaltes. *Journal of Raman Spectroscopy*, 35(11), 967-974.
- Kołodziejczak-Radzimska, A., & Jesionowski, T. (2014). Zinc oxide—from synthesis to application: a review. *Materials*, 7(4), 2833-2881. <https://doi.org/10.3390/ma7042833>
- Kumar, P., Kumar, S., Tapwal, A., & Thakur, N. (2024a). Chemical/green synthesized cobalt/copper-doped α -Fe₂O₃ nanoparticles: potential for environmental remediation. *Journal of Materials Research*, 39(5), 836-849. <https://doi.org/10.1557/s43578-023-01274-5>
- Kumar, P., Pathak, D. & Thakur, N. Trimetallic doped hematite (α -Fe₂O₃) (2024b). Nanoparticles using biomolecules of *Azadirachta indica* leaf extract for photocatalytic dye removal: insights into catalyst stability and reusability. *emergent mater.* . <https://doi.org/10.1007/s42247-024-00742-w>.
- Kumar, P., Tapwal, A., Kumar, S., & Thakur, N. (2024c). Improved photocatalytic and free radical scavenging studies of synthesized polymer PVP/*Azadirachta indica* leave extract-mediated Ni-Zn doped hematite nanoparticles. *Advances in Natural Sciences: Nanoscience and Nanotechnology*, 15(2), 025014. Doi: 10.1088/2043-6262/ad50bb
- Kumar, P., Thakur, N., Kumar, K., Kumar, S., Dutt, A., Thakur, V. K., ...& Thakur, N. (2024d). Catalyzing innovation: Exploring iron oxide nanoparticles-Origins, advancements, and future application horizons. *Coordination Chemistry Reviews*, 507, 215750. <https://doi.org/10.1016/j.ccr.2024.215750>
- Madan, H. R., Sharma, S. C., Suresh, D., Vidya, Y. S., Nagabhushana, H., Rajanaik, H., ... & Maiya, P. S. (2016). Facile green fabrication of nanostructure ZnO plates, bullets, flower, prismatic tip, closed pine cone: their antibacterial, antioxidant, photoluminescent and photocatalytic properties. *Spectrochimica Acta Part A: Molecular and Biomolecular Spectroscopy*, 152, 404-416. <https://doi.org/10.1016/j.saa.2015.07.067>
- Mahendra, C., Murali, M., Manasa, G., Ponnamma, P., Abhilash, M. R., Lakshmeesha, T. R., ...& Sudarshana, M. S. (2017). Antibacterial and antimutagenic potential of bio-fabricated zinc oxide nanoparticles of *Cochlospermum religiosum* (L.). *Microbial pathogenesis*, 110, 620-629. <https://doi.org/10.1016/j.micpath.2017.07.051>
- Malaikozhundan, B., Vaseeharan, B., Vijayakumar, S., Pandiselvi, K., Kalanjiam, M. A. R., Murugan, K., & Benelli, G. (2017). Biological therapeutics of Pongamiapinnata coated zinc oxide nanoparticles against clinically important pathogenic bacteria, fungi and MCF-7 breast cancer cells. *Microbial pathogenesis*, 104, 268-277. <https://doi.org/10.1016/j.micpath.2017.01.029>
- Maslowsky Jr, E. (2019). *Vibrational spectra of organometallics: theoretical and experimental data*. John Wiley & Sons.
- Mirza, A. U., Kareem, A., Nami, S. A., Bhat, S. A., Mohammad, A., & Nishat, N. (2019). Maluspumila and Juglenregia plant species mediated zinc oxide nanoparticles: synthesis, spectral characterization, antioxidant and antibacterial studies. *Microbial pathogenesis*, 129, 233-241. <https://doi.org/10.1016/j.micpath.2019.02.020>
- Mobarak, M. B., Hossain, M. S., Yeasmin, Z., Mahmud, M., Rahman, M. M., Sultana, S., ...& Ahmed, S. (2022). Probing the photocatalytic competency of hydroxyapatite synthesized by solid state and wet chemical precipitation method. *Journal of Molecular Structure*, 1252, 132142. <https://doi.org/10.1016/j.molstruc.2021.132142>

- Pai, S., Sridevi, H., Varadavenkatesan, T., Vinayagam, R., & Selvaraj, R. (2019). Photocatalytic zinc oxide nanoparticles synthesis using *Peltophorumpterocarpum* leaf extract and their characterization. *Optik*, 185, 248-255. <https://doi.org/10.1016/j.ijleo.2019.03.101>
- Prakasham, R. S., Kumar, B. S., Kumar, Y. S., & Kumar, K. P. (2014). Production and characterization of protein encapsulated silver nanoparticles by marine isolate *Streptomyces parvulus* SSNP11. *Indian journal of microbiology*, 54, 329-336. <https://doi.org/10.1007/s12088-014-0452-1>
- Prasad, K. S., Prasad, S. K., Veerapur, R., Lamraoui, G., Prasad, A., Prasad, M. N., ...& Shivamallu, C. (2021). Antitumor potential of green synthesized ZnONPs using root extract of *Withaniasomnifera* against human breast cancer cell line. *Separations*, 8(1), 8. <https://doi.org/10.3390/separations8010008>
- Qidwai, A., Pandey, A., Kumar, R., Shukla, S. K., & Dikshit, A. (2018). Advances in biogenic nanoparticles and the mechanisms of antimicrobial effects. *Indian Journal of Pharmaceutical Sciences*, 80(4).
- Rajabi, H. R., Naghiha, R., Kheirizadeh, M., Sadatfaraji, H., Mirzaei, A., & Alvand, Z. M. (2017). Microwave assisted extraction as an efficient approach for biosynthesis of zinc oxide nanoparticles: synthesis, characterization, and biological properties. *Materials Science and Engineering: C*, 78, 1109-1118. <https://doi.org/10.1016/j.msec.2017.03.090>
- Rajendran, N. K., George, B. P., Houreld, N. N., & Abrahamse, H. (2021). Synthesis of zinc oxide nanoparticles using *Rubusfairholmianus* root extract and their activity against pathogenic bacteria. *Molecules*, 26(10), 3029. <https://doi.org/10.3390/molecules26103029>
- Ramya, V., Kalaiselvi, V., Kannan, S. K., Shkir, M., Ghramh, H. A., Ahmad, Z., ...& Vidhya, N. (2022). Facile synthesis and characterization of zinc oxide nanoparticles using *Psidiumguajava* leaf extract and their antibacterial applications. *Arabian Journal for Science and Engineering*, 47(1), 909-918. <https://doi.org/10.1007/s13369-021-05717-1>
- Rana, A., Kumar, P., Thakur, N., Kumar, S., Kumar, K., & Thakur, N. (2024). Investigation of photocatalytic, antibacterial and antioxidant properties of environmentally green synthesized zinc oxide and yttrium doped zinc oxide nanoparticles. *Nano-Structures & Nano-Objects*, 38, 101188. <https://doi.org/10.1016/j.nanoso.2024.101188>
- Rehan, M., Ahmed-Farid, O. A., Ibrahim, S. R., Hassan, A. A., Abdelrazek, A. M., Khafaga, N. I., & Khattab, T. A. (2019). Green and sustainable encapsulation of Guava leaf extracts (*Psidiumguajava* L.) into alginate/starch microcapsules for multifunctional finish over cotton gauze. *ACS sustainable chemistry & engineering*, 7(22), 18612-18623. <https://doi.org/10.1021/acs.iecr.4c01969>
- Ren, F., Xin, R., Ge, X., & Leng, Y. (2009). Characterization and structural analysis of zinc-substituted hydroxyapatites. *Actabiomaterialia*, 5(8), 3141-3149. <https://doi.org/10.1016/j.actbio.2009.04.014>
- Rouhi, J., Mahmud, S., Naderi, N., Ooi, C. R., & Mahmood, M. R. (2013). Physical properties of fish gelatin-based bio-nanocomposite films incorporated with ZnO nanorods. *Nanoscale research letters*, 8, 1-6. <https://doi.org/10.1186/1556-276X-8-364>
- Ruangtong, J., Jiraroj, T., & T-Thienprasert, N. P. (2020). Green synthesized ZnO nanosheets from banana peel extract possess anti-bacterial activity and anti-cancer activity. *Materials Today Communications*, 24, 101224. <https://doi.org/10.1016/j.mtcomm.2020.101224>
- Saha, R., Subramani, K., Raju, S. A. K. P. M., Rangaraj, S., & Venkatachalam, R. (2018). *Psidiumguajava* leaf extract-mediated synthesis of ZnO nanoparticles under different processing parameters for hydrophobic and antibacterial finishing over cotton fabrics. *Progress in Organic Coatings*, 124, 80-91. <https://doi.org/10.1016/j.porgcoat.2018.08.004>

- Samat, N. A., & Nor, R. M. (2013). Sol-gel synthesis of zinc oxide nanoparticles using Citrus aurantifolia extracts. *Ceramics International*, 39, S545-S548. <https://doi.org/10.1016/j.ceramint.2012.10.132>
- Sharma, S., & Kumar, K. (2021). Aloe-vera leaf extract as a green agent for the synthesis of CuO nanoparticles inactivating bacterial pathogens and dye. *Journal of Dispersion Science and Technology*, 42(13), 1950-1962. <https://doi.org/10.1080/01932691.2020.1791719>
- Siddiqi, K. S., Husen, A., & Rao, R. A. (2018). A review on biosynthesis of silver nanoparticles and their biocidal properties. *Journal of nanobiotechnology*, 16, 1-28. <https://doi.org/10.1186/s12951-018-0334-5>
- Singhai, M., Chhabra, V., Kang, P., & Shah, D. O. (1997). Synthesis of ZnO nanoparticles for varistor application using Zn-substituted aerosol OT microemulsion. *Materials Research Bulletin*, 32(2), 239-247. [https://doi.org/10.1016/S0025-5408\(96\)00175-4](https://doi.org/10.1016/S0025-5408(96)00175-4)
- Song, J. Y., & Kim, B. S. (2008). Biological synthesis of bimetallic Au/Ag nanoparticles using Persimmon (Diopyros kaki) leaf extract. *Korean Journal of Chemical Engineering*, 25, 808-811. <https://doi.org/10.1007/s11814-008-0133-z>
- Sukri, S. N. A. M., Shameli, K., Wong, M. M. T., Teow, S. Y., Chew, J., & Ismail, N. A. (2019). Cytotoxicity and antibacterial activities of plant-mediated synthesized zinc oxide (ZnO) nanoparticles using Punicagranatum (pomegranate) fruit peels extract. *Journal of Molecular Structure*, 1189, 57-65. <https://doi.org/10.1016/j.molstruc.2019.04.026>
- Sun, J. H., Dong, S. Y., Feng, J. L., Yin, X. J., & Zhao, X. C. (2011). Enhanced sunlight photocatalytic performance of Sn-doped ZnO for Methylene Blue degradation. *Journal of Molecular Catalysis A: Chemical*, 335(1-2), 145-150. <https://doi.org/10.1016/j.molcata.2010.11.026>
- Thakur, N., & Thakur, N. (2024a). Degradation of textiles dyes and scavenging activity of spherical shape obtained anatase phase of Co-Ni-doped TiO₂ nanocatalyst. *Journal of Materials Science: Materials in Electronics*, 35(2), 134. <https://doi.org/10.1007/s10854-023-11851-3>
- Thakur, N., & Thakur, N. (2024b). Photocatalytic adsorption and scavenging potential of chemical and green encapsulated anatase phase of coupled doped Zn-Co TiO₂ nanoparticles. *Journal of Dispersion Science and Technology*, 1-16. <https://doi.org/10.1080/01932691.2024.2312841>
- Thakur, N., Thakur, N., Kumar, A., Thakur, V. K., Kalia, S., Arya, V., ...& Kyzas, G. Z. (2024c). A critical review on the recent trends of photocatalytic, antibacterial, antioxidant and nanohybrid applications of anatase and rutile TiO₂ nanoparticles. *Science of The Total Environment*, 169815. <https://doi.org/10.1016/j.scitotenv.2023.169815>
- Thakur, S., Kumar, P., Thakur, N., Kumar, K., Jeet, K., Kumar, S., & Thakur, N. (2024d). Photocatalytic, antibacterial and antioxidant potential of spheroidal shape chromium and yttrium doped cobalt oxide nanoparticles: A green approach. *Journal of the Indian Chemical Society*, 101199. <https://doi.org/10.1016/j.jics.2024.101199>
- Thakur, N., Kumar, A., & Thakur, N. (2023). Tinosporacordifolia and polyvinylpyrrolidone encapsulated dual doped Ni-Cu TiO₂ emerging nanocatalyst for the removal of organic dyes from wastewater and its free radical assay activity. *Hybrid Advances*, 4, 100086. <https://doi.org/10.1016/j.hybadv.2023.100086>
- Verma, N., Pathak, D., & Thakur, N. (2024). Eco-friendly green synthesis of (Cu, Ce) dual-doped ZnO nanoparticles with Colocasiaesculenta plant extract using microwave assisted technique for antioxidant and antibacterial activity. *Next Materials*, 5, 100271. <https://doi.org/10.1016/j.nxmte.2024.100271>

Vijayakumar, S., Vaseeharan, B., Malaikozhundan, B., &Shobiya, M. (2016). Laurusnobilis leaf extract mediated green synthesis of ZnO nanoparticles: Characterization and biomedical applications. *Biomedicine & Pharmacotherapy*, 84, 1213-1222. <https://doi.org/10.1016/j.biopha.2016.10.038>

Zare, E., Pourseyedi, S., Khatami, M., &Darezereshki, E. (2017). Simple biosynthesis of zinc oxide nanoparticles using nature's source, and it's in vitro bio-activity. *Journal of Molecular Structure*, 1146, 96-103. <https://doi.org/10.1016/j.molstruc.2017.05.118>

Zhang, L., Gu, F. X., Chan, J. M., Wang, A. Z., Langer, R. S., &Farokhzad, O. C. (2008). Nanoparticles in medicine: therapeutic applications and developments. *Clinical pharmacology & therapeutics*, 83(5), 761-769. <https://doi.org/10.1038/sj.clpt.6100400>



'Publisher's note: Eurasia Academic Publishing Group (EAPG) remains neutral with regard to jurisdictional claims in published maps and institutional affiliations.

Open Access This article is licensed under a Creative Commons Attribution-NoDerivatives 4.0 International (CC BY-ND 4.0) licence, which permits copying and redistributing the material in any medium or format for any purpose, even commercially. The licensor cannot revoke these freedoms as long as you follow the licence terms. Under the following terms, you must give appropriate credit, provide a link to the license, and indicate if changes were made. You may do so in any reasonable manner, but not in any way that suggests the licensor endorsed you or your use. If you remix, transform, or build upon the material, you may not distribute the modified material.

To view a copy of this license, visit <https://creativecommons.org/licenses/by-nd/4.0/>.